

Invited Article: Electrically tunable silicon-based on-chip microdisk resonator for integrated microwave photonic applications

Weifeng Zhang and Jianping Yao

Citation: *APL Photonics* **1**, 080801 (2016); doi: 10.1063/1.4961685

View online: <http://dx.doi.org/10.1063/1.4961685>

View Table of Contents: <http://scitation.aip.org/content/aip/journal/app/1/8?ver=pdfcov>

Published by the [AIP Publishing](#)

Articles you may be interested in

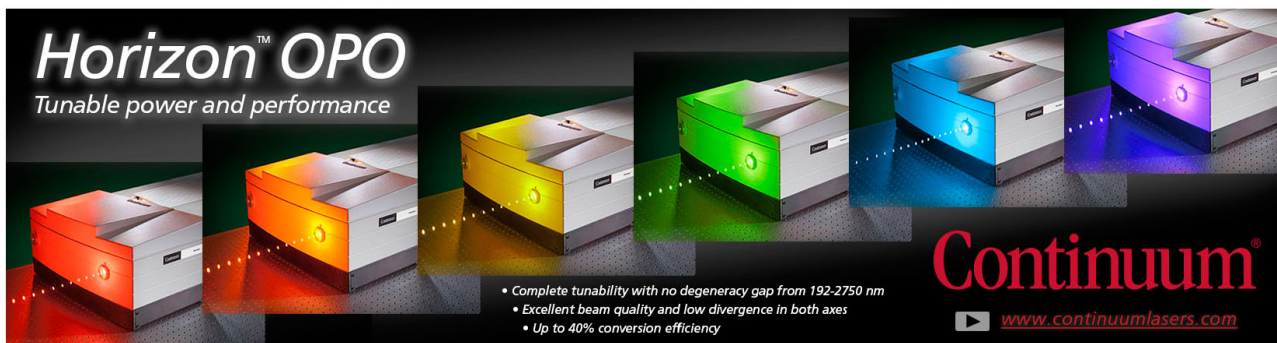
[Fine-tuning of whispering gallery modes in on-chip silica microdisk resonators within a full spectral range](#)
Appl. Phys. Lett. **102**, 041104 (2013); 10.1063/1.4789755

[Tuning the coherent interaction in an on-chip photonic-crystal waveguide-resonator system](#)
Appl. Phys. Lett. **97**, 101102 (2010); 10.1063/1.3486686

[Tunable silicon microring resonator with wide free spectral range](#)
Appl. Phys. Lett. **89**, 071110 (2006); 10.1063/1.2337162

[On-chip microfluidic tuning of an optical microring resonator](#)
Appl. Phys. Lett. **88**, 111107 (2006); 10.1063/1.2182111

[APL Photonics](#)



Horizon™ OPO
Tunable power and performance

• Complete tunability with no degeneracy gap from 192-2750 nm
• Excellent beam quality and low divergence in both axes
• Up to 40% conversion efficiency

Continuum®
www.continuumlasers.com

The advertisement features a row of five Continuum Horizon OPO units, each emitting a different color of laser light: red, orange, yellow, green, and blue. The units are shown from a three-quarter perspective, highlighting their compact, boxy design. The background is dark, making the glowing units stand out.

Invited Article: Electrically tunable silicon-based on-chip microdisk resonator for integrated microwave photonic applications

Weifeng Zhang and Jianping Yao^a

Microwave Photonic Research Laboratory, School of Electrical Engineering and Computer Science, University of Ottawa, 25 Templeton Street, Ottawa, Ontario K1N 6N5, Canada

(Received 24 May 2016; accepted 15 August 2016; published online 29 August 2016)

Silicon photonics with advantages of small footprint, compatibility with the mature CMOS fabrication technology, and its potential for seamless integration with electronics is making a significant difference in realizing on-chip integration of photonic systems. A microdisk resonator (MDR) with a strong capacity in trapping and storing photons is a versatile element in photonic integrated circuits. Thanks to the large index contrast, a silicon-based MDR with an ultra-compact footprint has a great potential for large-scale and high-density integrations. However, the existence of multiple whispering gallery modes (WGMs) and resonance splitting in an MDR imposes inherent limitations on its widespread applications. In addition, the waveguide structure of an MDR is incompatible with that of a lateral PN junction, which leads to the deprivation of its electrical tunability. To circumvent these limitations, in this paper we propose a novel design of a silicon-based MDR by introducing a specifically designed slab waveguide to surround the disk and the lateral sides of the bus waveguide to suppress higher-order WGMs and to support the incorporation of a lateral PN junction for electrical tunability. An MDR based on the proposed design is fabricated and its optical performance is evaluated. The fabricated MDR exhibits single-mode operation with a free spectral range of 28.85 nm. Its electrical tunability is also demonstrated and an electro-optic frequency response with a 3-dB modulation bandwidth of ~ 30.5 GHz is measured. The use of the fabricated MDR for the implementation of an electrically tunable optical delay-line and a tunable fractional-order temporal photonic differentiator is demonstrated. © 2016 Author(s). All article content, except where otherwise noted, is licensed under a Creative Commons Attribution (CC BY) license (<http://creativecommons.org/licenses/by/4.0/>). [<http://dx.doi.org/10.1063/1.4961685>]

Silicon photonics, due to its small footprint, compatibility with the current CMOS technology, and its potential for seamless integration with electronics, is considered a promising photonic integration platform.¹ Recently, there has been an ever-increasing interest in studying the use of the silicon photonic technology to realize on-chip integration of microwave photonic systems, which would largely enhance the system performance and reduce the power consumption.^{2,3} To achieve integrated microwave photonic (IMWP) systems with a large-scale and high-density integration, it is highly preferred that the on-chip components have a compact footprint. Thanks to its ultra-compact size and strong light-confining capacity, an on-chip optical microcavity holds a significant potential for IMWP applications. As an optical microcavity, a silicon-based microring resonator (MRR) has been extensively researched and found numerous applications in IMWP.⁴ For example, an MRR has been used to realize a photonic temporal differentiator.⁵ An MRR or multiple cascaded MRRs have also been used as an integrated optical delay line.^{6,7} By incorporating a PN junction in the waveguide of an MRR, a high-speed MRR-based electro-optic modulator has been demonstrated⁸ and employed for the implementation of a photonic temporal differentiator with a

^aElectronic mail: jpyao@eecs.uottawa.ca.



tunable fractional order.⁹ A microdisk resonator (MDR), also an optical microcavity, exhibits better performance in terms of footprint and light-confining capacity over an MRR.^{10,11} Although some demonstrations using an MDR to achieve microwave photonic phase shift or microwave photonic generation have been reported,¹²⁻¹⁴ compared with an MRR, an MDR is much less used due to some inherent limitations. First, an MDR supports multiple whispering gallery modes (WGMs), which are not desired especially for filtering applications where the free spectral range (FSR) should be large to have a large finesse. Second, resonance-splitting exists in an MDR, which is resulted from the scattering induced by the sidewall roughness. Due to the resonance-splitting, the spectral response of an MDR with an ideal Lorentzian-shape is distorted, which is unwanted for filtering applications. Third, the structure of an MDR is not compatible with that of a lateral PN junction. Therefore, it is challenging to achieve an electrically tunable MDR in which a lateral PN junction is essential. Although an electrically tunable MDR by incorporating an unusual vertical PN junction¹⁵ or using a complicated disk configuration¹⁶ has been reported, the structures are very complicated which would heavily increase the fabrication cost.

To overcome the limitations and to make an MDR suitable for IMWP applications, in this paper, we propose a novel design of a silicon-based on-chip MDR by introducing a specifically designed slab waveguide to surround the disk and the lateral sides of the bus waveguide to suppress the higher-order WGMs and to support the incorporation of a lateral PN junction for electrical tunability. First, the higher-order WGMs have a tendency to couple into a leaky mode by incorporating a slab waveguide to surround the disk, which enables a single-mode operation. In addition, the introduction of a slab waveguide would make part of the sidewall further away from the fundamental WGM, which could weaken the scattering resulted from the sidewall roughness, and help alleviate the resonance-splitting. Furthermore, in a conventional MDR, it is impossible to implement a lateral PN junction since the center of the fundamental WGM is too close to the edge of the disk which gives an area that is not sufficiently large to make a PN junction. Thanks to the introduction of the slab waveguide in the proposed work, the area is increased which allows the implementation of a lateral PN junction.

The proposed MDR is designed, fabricated, and its optical performance is experimentally evaluated. The results show that the MDR exhibits a single-mode operation with a free spectral range (FSR) of 28.85 nm. No resonance-splitting is observed in its resonances. The electrical tunability is also demonstrated and an electro-optic frequency response with a 3-dB modulation bandwidth as wide as ~30.5 GHz is measured. These properties make the fabricated MDR highly suitable for microwave photonics applications. In this paper, the use of the fabricated MDR for the implementation of an electrically tunable optical delay-line with a tunable time delay as large as 72 ps and a tunable fractional-order temporal photonic differentiator with a tunable differentiation order from 0.38 to 1.53 is demonstrated.

Fig. 1(a) illustrates the perspective view of an electrically tunable silicon-based on-chip MDR. It has an all-pass configuration consisting of a bus waveguide and a disk. To clearly illustrate the internal structure of the device, the cladding layer of silica is removed. As can be seen, the proposed MDR has a specifically designed slab waveguide to surround the disk and the lateral sides of the bus waveguide. The employment of the slab waveguide aims to suppress the higher-order WGMs by coupling into leaky modes to have a single-mode operation and to enable the incorporation of a lateral PN junction to achieve the electrical tunability of the MDR. In addition, the introduction of the slab waveguide makes part of the sidewall further away from the confined mode, which would weaken the scattering resulted from the sidewall roughness. This helps alleviate the resonance-splitting. To make the design to be compliant with the design rules, the slab waveguide is designed to have a special profile. Near the lateral sides of the bus waveguide, the widths of the slab waveguide are kept identical. Near the disk, in order to support the incorporation of a lateral PN junction, the slab waveguide is designed to have a semicircle profile to wrap the disk. Fig. 1(b) shows the top-view of the MDR. To make the disk have one resonance wavelength near 1550 nm in the C band, the disk is designed to have a radius of 3.7 μm and the slab waveguide has a radius of 9.2 μm . The lateral PN junction is formed along the edge of the disk. Since the plasma dispersion effect is more sensitive to the change of the free-hole concentration, in order to increase the tuning efficiency by increasing the overlap between the confined light mode with the p-type doping

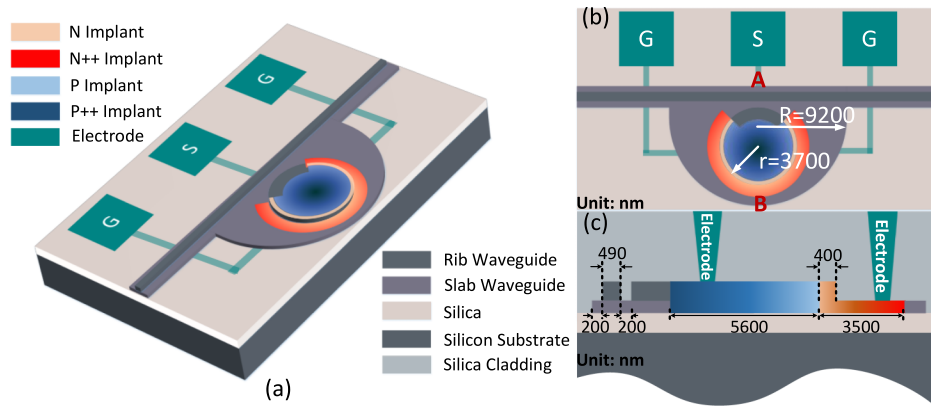


FIG. 1. (a) Perspective view of an electrically tunable silicon-based on-chip MDR. (b) Top view of the proposed MDR. (c) Cross-sectional view of the planar structure along the direction from A to B on (b).

region, most of the disk is designed to be p-type doped, while the edge of the disk and the slab waveguide are n-type doped. To guarantee that the doping does not deteriorate the optical coupling between the bus waveguide and the disk, there is no doping along the arc with an angle of 120° near the coupling region, as shown in Fig. 1(b). In addition, three contact windows are opened on the silica pads, with a $2\text{-}\mu\text{m}$ -thick aluminum layer deposited to make the contacts. Fig. 1(c) illustrates the cross-sectional view of the planar structure along the direction from A to B in Fig. 1(b). To meet the phase-matching condition for optical coupling between the bus waveguide and the disk which requires that the effective refractive index of the fundamental TE mode supported by the bus waveguide is equal to that of the fundamental WGM supported by the disk, the bus waveguide is designed to have a specific width of 490 nm. The coupling gap has a width of 200 nm. To optimize the tuning efficiency, the overlap between the PN junction and the fundamental WGM is maximized by slightly shifting the center of the PN junction inward by 400 nm from the edge of the disk. To minimize the heavy doping induced absorption loss, additional p++ and n++ implantations, $1\ \mu\text{m}$ away from the center of the PN junction, are utilized for ohmic contact formation. The proposed MDR is fabricated using a standard fabrication process of 248-nm deep ultraviolet lithography at IME, Singapore. Since a standard fabrication process is employed, the fabrication cost especially for high volume production is greatly reduced.

Fig. 2(a) shows the electrical field amplitude of the fundamental WGM at 1546 nm evaluated in the x - y plane of the proposed MDR. The dotted black line depicts the profile of the disk. As can be seen, the center of the mode has a distance of 400 nm from the edge of the disk, which perfectly matches the slightly shifted PN junction. In addition, by using the equation $n_{\text{eff}} = m\lambda_0/2\pi R$, where λ_0 is the resonance wavelength, m is the azimuth harmonic number of the WGM, and R is the disk radius, the effective refractive index of the individual WGM supported by the MDR can be

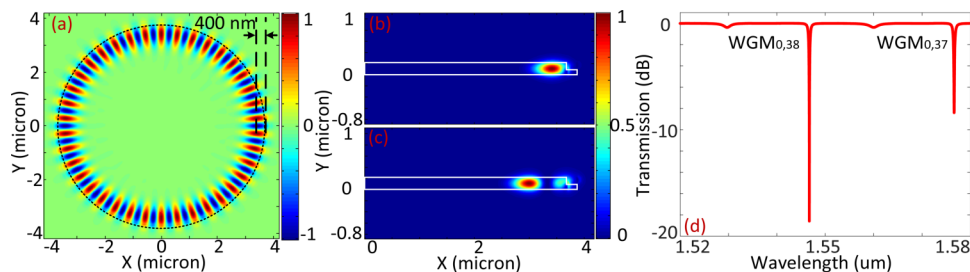


FIG. 2. Simulation results: (a) electrical field amplitude of the fundamental WGM at 1546 nm evaluated in the x - y plane at the center of the proposed disk; (b) electrical field profile of the fundamental radial TE mode in the proposed disk; (c) electrical field profile of the first-order radial TE mode in the proposed disk; and (d) transmission spectrum.

calculated, which could be employed to calculate the width of the bus waveguide to meet the phase-matching condition. Fig. 2(b) illustrates the electrical field profile of the fundamental radial TE mode supported by the MDR. It is clear to see that the fundamental TE radial mode decays rapidly in the radial direction. Thanks to the slab waveguide, part of the sidewall is further away from the confined mode, which would help weaken the scattering resulted from the sidewall roughness. This helps alleviate the resonance-splitting. Moreover, the energy profile of the fundamental radial TE mode exhibits an energy tail outside the disk, which would strengthen the optical coupling between the bus waveguide and the disk. Fig. 2(c) illustrates the electrical field profile of the first-order radial TE mode supported by the MDR. Compared with the fundamental radial TE mode, the first-order radial TE mode has a much stronger energy tail, which leads to its coupling into a leaky mode. Fig. 2(d) shows the simulated transmission spectrum of the proposed MDR. As can be seen, the MDR has a simple and clear transmission spectrum which presents a single-mode operation. Each notch in the spectrum represents a specific $\text{WGM}_{p,q}$ resonance in which p and q are the radial and azimuthal harmonic numbers. The higher-order WGMs are effectively suppressed, which is enabled because the width of the bus waveguide is specifically designed to excite the fundamental WGM in the disk, and the introduction of the slab waveguide makes the higher-order modes have a tendency to couple the light into the leaky mode. Note that in the simulation, the sidewall roughness is not considered.

Fig. 3(a) shows the image of the fabricated MDR captured by a microscope camera. Two TE-mode grating couplers with a center-to-center space of $254 \mu\text{m}$ are used to couple light between the chip and the input and output fibers. To minimize the chip footprint and to reduce the bending loss, a strip waveguide is mostly used to guide the lightwave signal. Since the bus waveguide in the electrically tunable MDR has a slab waveguide, which is different from the strip waveguide, a double-layer linear taper waveguide with a length of $50 \mu\text{m}$ is used for the mode transition between the strip waveguide and the bus waveguide. The entire device is $167 \mu\text{m}$ in length and $230 \mu\text{m}$ in width, giving an ultra-compact footprint of 0.384 mm^2 . Fig. 3(b) shows the zoom-in view of the disk. This small radius of the disk has an exceptional advantage in achieving high-density integration and reducing the power consumption. The optical performance of the fabricated MDR is first evaluated using an optical vector analyzer (LUNA OVA CTe) to measure its transmission spectrum. Fig. 3(c) shows the measured transmission spectrum when a zero bias voltage is applied, which exhibits a single-mode operation. Each notch in the spectrum represents a resonance wavelength and the FSR is estimated to be 28.85 nm , which ensures that in the C band, there is only one resonance wavelength. This simple and clear transmission spectrum matches well with the simulation result in Fig. 2(d) except that the resonance wavelength is shifted due to the fabrication errors, and the high-order WMG modes are completely suppressed due to the sidewall roughness induced

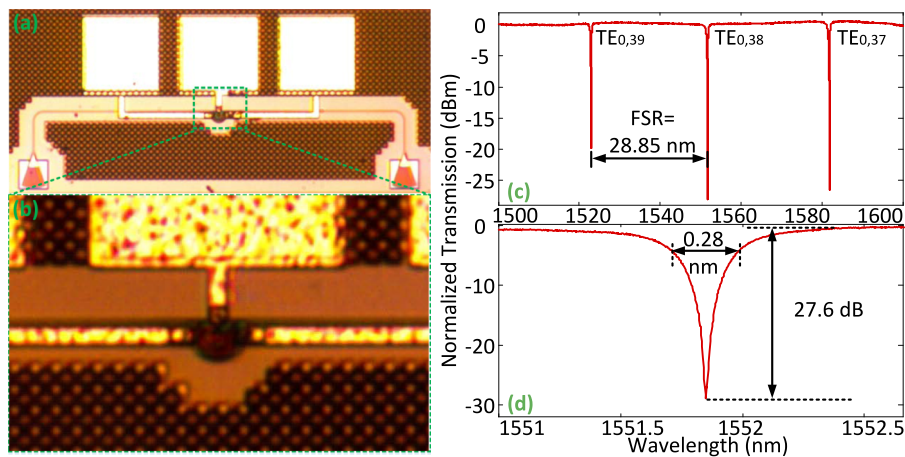


FIG. 3. (a) Image of the fabricated MDR, (b) zoom-in view of the microdisk, (c) measured transmission spectrum of the fabricated MDR, and (d) zoom-in view of the resonance of the fabricated MDR at the wavelength of 1551.84 nm .

scattering loss. The insertion loss of the fabricated MDR is measured to be 13 dB, most of which is caused by the fiber-to-fiber I/O coupling loss. By optimizing the design of the grating couplers, the insertion loss would be largely reduced. In addition, no resonance-splitting is observed at a high wavelength resolution of 2.4 pm, which confirms that the introduction of the slab waveguide weakens the scattering resulted from the sidewall roughness. Fig. 3(d) shows the zoom-in view of the resonance $WGM_{0,38}$, of which the resonance wavelength is located at 1551.84 nm. The resonance has a 3-dB bandwidth of 280 pm with a Q-factor of 5,500 and an extinction ratio of 27.6 dB.

Then, the DC performance of the fabricated MDR is evaluated when the PN junction is reverse biased. To clearly illustrate the optical performance change when a bias voltage is applied, we show in detail the wavelength shift of the notch at the resonance $WGM_{0,38}$. Fig. 4(a) shows the measured voltage-current (V-I) curve of the PN junction when reverse biased. As can be seen, the PN junction reaches breakdown at approximately 15.7 V. Fig. 4(b) shows that the notch shift as the bias voltage is increasing. When reverse biased, as the voltage is increasing, more free carriers are extracted and the depletion region is widened. Thus, based on the plasma dispersion effect, the effective refractive index of the waveguide is increased which would lead to a red-shifted of the spectrum. In the meanwhile, the decrease in the number of free carriers would reduce the free-carrier induced absorption loss, which could elevate the Q-factor, and the extinction ratio is also improved since the coupling condition is reaching the critical condition. For example, when biased at 19 V, the injection current is measured to 500 nA. From the measured resonance spectrum, the Q-factor is increased to 7,050, the extinction ratio is increased to 37.3 dB, and the notch wavelength is red-shifted by 94 pm.

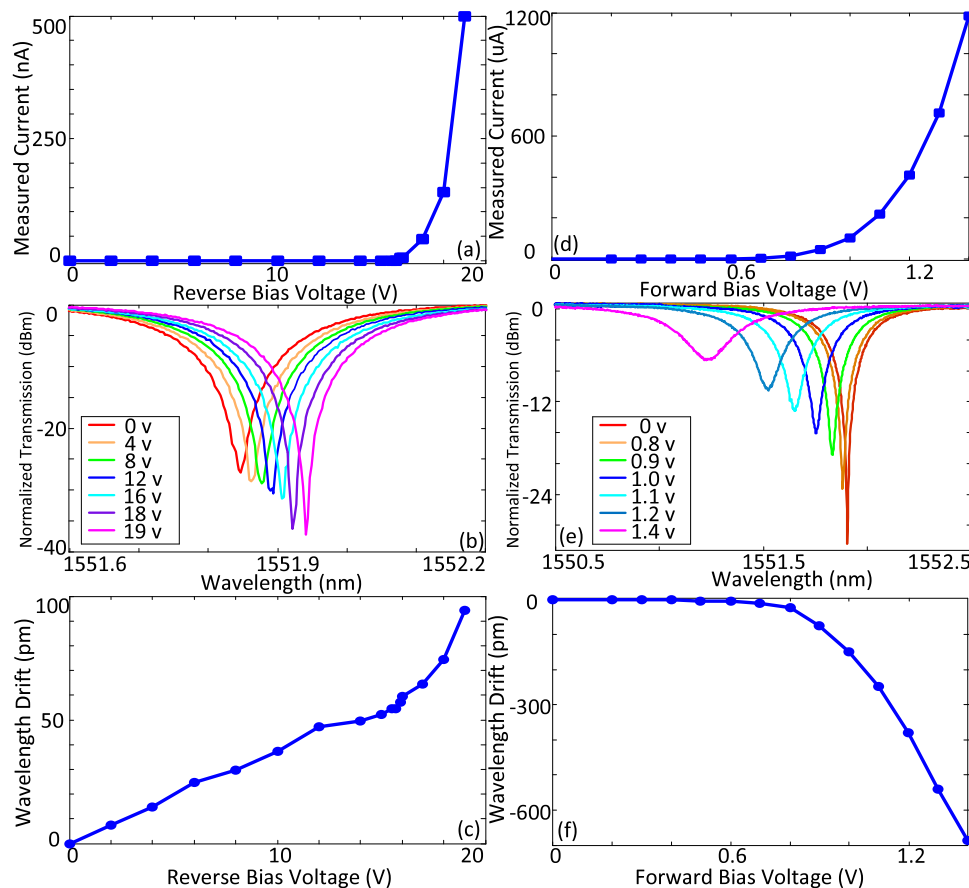


FIG. 4. Measurement results for the PN junction being reverse biased: (a) measured V-I curves of the PN junction, (b) wavelength shift of the resonance $WGM_{0,38}$, and (c) wavelength shift when the bias voltage is increased. Measurement results for the PN junction being forward biased: (d) measured V-I curves of the PN junction, (e) wavelength shift of the resonance $WGM_{0,38}$, and (f) wavelength shift when the bias voltage is increased.

Fig. 4(c) shows the tuning of the spectral response, which gives a wavelength shift rate of 4.4 pm/V. Then, the DC performance of the fabricated MDR is evaluated for the PN junction being forward biased. Fig. 4(d) shows the V-I curve of the PN junction when forward biased, which indicates that the junction is turned on at about -0.8 V. Fig. 4(e) shows a blue-shift of the notch as the forward voltage is increasing. The blue shift is resulted from the decrease in the refractive index induced by the free-carrier injection. In addition, the injected free-carrier would also introduce an excess absorption loss, which would degrade the performance of the fabricated MDR. As can be seen in Fig. 4(e), when the bias voltage is increasing, the Q-factor and the extinction ratio are reduced. For a current of 1.2 mA when biased at -1.4 V, the Q-factor is reduced to 3880 and the extinction ratio is reduced to 8.6 dB. The blue shift of the notch wavelength is found to be 0.67 nm. Fig. 4(f) shows the tuning of the spectral response which gives a wavelength shift rate of -1.15 nm/V after the PN junction is turned on. When a bias voltage is applied on the fabricated MDR, the notch could be shifted, which could find applications as a tunable optical filter.¹⁷ To improve the Q-factor of the MDR for high wavelength selectivity as an optical filter, one solution is to increase the radius of the disk. To have a filter with a flat-top, a design of cascaded MDRs with specifically designed coupling gaps could be employed.

The AC performance of the fabricated MDR is evaluated using a vector network analyzer (Agilent E8364A) to measure its electro-optic frequency response. Since the light-confinement resonating structure of the optical microcavity can enhance the effect of refractive index change, the electrically tunable MDR can be used to perform electro-optic modulation.¹⁸ For a silicon microdisk modulator, its 3-dB modulation bandwidth depends on the RC time of the reverse-biased PN junction and the photon lifetime of the cavity. The photon lifetime is determined by the Q factor of the cavity, given by $\tau = Q\lambda_0/2\pi c$, where c is the speed of light in vacuum. Based on the estimated Q-factor of the fabricated MDR, the photon-lifetime determined cutoff frequency is calculated to be 35.1 GHz according to $f_\tau = 1/2\pi\tau$. Fig. 5 shows the measured electro-optic frequency response for a reverse bias voltage tuned from 0 V to 0.9 V when the wavelength of the input light is chosen to be 1551.81 nm in the linear regime. At a bias voltage of 0 V, the 3-dB modulation bandwidth is measured to be 5 GHz, and at a bias voltage of 0.9 V, the 3-dB modulation bandwidth is measured to be 30.5 GHz. As can be found, with the reverse bias voltage increasing from 0 to 0.9 V, the 3-dB modulation bandwidth is increased from 5 to 30.5 GHz. This is because the red-shift of the resonance induced by the increase in the reverse bias voltage changes the photon-lifetime of the input wavelength. As the reverse bias voltage is increasing, the resonance is red-shifted, while the input wavelength keeps unchanged, which makes the resonance wavelength further away from the input wavelength. Since the photon lifetime of the cavity is wavelength-dependent, at the resonance wavelength, the light-confinement capacity of the cavity is strongest and the photon lifetime is longest. Therefore, the red-shift would lead to a weaker confinement capability of the cavity for the input wavelength and its corresponding photon lifetime is becoming shorter. Thus, the measured 3-dB modulation bandwidth is becoming larger. This photon-lifetime-dependent electro-optic frequency response confirms that the modulation bandwidth of the fabricated MDR is mainly limited by the photon lifetime of the cavity. Compared to a well-developed silicon microring

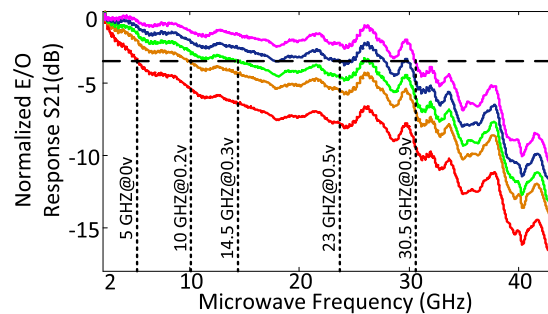


FIG. 5. Measured electro-optic frequency response for a reverse bias voltage tuned from 0 V to 0.9 V when the wavelength of the input light is chosen to be 1551.81 nm in the linear regime.

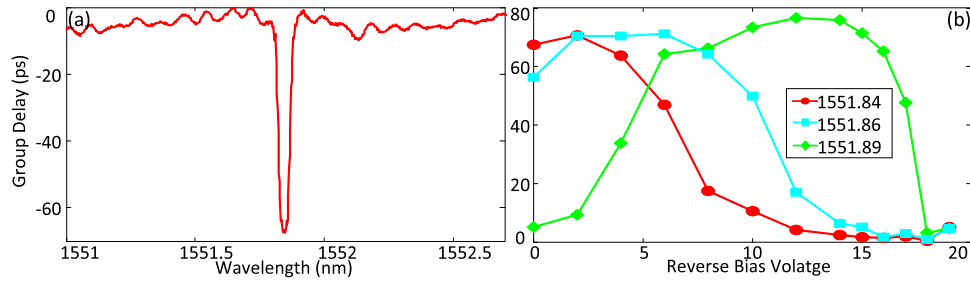


FIG. 6. (a) Measured group delay of the resonance WGM_{0,38} in the fabricated MDR and (b) electrical tunability of the group delay at three different wavelengths.

modulator, the fabricated MDR has an equivalent capacity of high-speed electro-optic modulation but an ultra-compact footprint, which indicates smaller power consumption and significant potential for the applications in the chip-to-chip interconnect.¹⁹

Thanks to the light-confinement capacity, an on-chip microcavity has a strong dispersion near the resonance and thus a large group delay. Recently, an on-chip microcavity has been well studied to realize an optical delay line, which could find important applications in microwave photonic delay-line filtering and optical true-time delay beamforming. For example, an MRR or multiple cascaded MRRs have been used for the implementation of an optical delay line. However, the comparatively large size and the relatively weak dispersion of an MRR would make the footprint of the delay line quite larger. To reduce the footprint, an MDR with a stronger dispersion near the resonance is a good candidate to realize an integrated optical delay line. Fig. 6(a) illustrates the measured group delay of the resonance WGM_{0,38} in the fabricated MDR. As can be seen, the MDR presents a very large group delay of 68 ps. The ultra-compact footprint with a strong group delay fully demonstrates its potential in realizing an on-chip optical delay line. Fig. 6(b) shows the electrical tunability of the group delay at three different wavelengths. As the reverse bias voltage is increasing, the group delays at the three different wavelengths give different changes. For example, at 1551.84 nm, shown in the red line, as the bias voltage increases, the time delay is first increased to 72 ps from 68 ps at a bias voltage of 0 V and then is decreased to zero when the bias voltage is larger than 15 V. Such a change is resulted from the shift of the resonance at different bias voltages, which demonstrates the electrical tunability of the time delay. Again, the ultra-compact footprint, the large group delay, and the flexible electrical tunability make an MDR a better option in realizing an on-chip optical delay line. Note that for an optical delay line, a wider operation width is always preferred. By series-double-coupling several MDRs, a delay line with a wider bandwidth could be achieved.²⁰

Photonic processing of microwave signals is a topic of interest in microwave photonics. A photonic temporal differentiator, as one of the basic signal processing blocks, is used to perform temporal differentiation of the complex envelope of an arbitrary optical signal.²¹ In general, a photonic temporal differentiator can be realized using an optical system that has a transfer function given by $[j(\omega - \omega_0)]^n$, where n is the differentiation order, ω is the optical frequency, and ω_0 is the optical carrier frequency. When the differentiation order n is not one, the operator is generalized to be a fractional-order photonic temporal differentiator.²² MRRs have been intensively investigated in realizing the photonic temporal differentiation. To verify that the fabricated MDR can be used to implement a photonic temporal differentiator with a tunable differentiation order, an experiment based on the setup shown in Fig. 7(a) is performed. A short Gaussian pulse from a tunable mode locked laser (TMLL) is sent to a WaveShaper to shape the Gaussian pulse to have a temporal full width at half maximum (FWHM) of 500 ps. A polarization controller (PC) is used to adjust the polarization state of the input signal to minimize the polarization-dependent loss. The differentiated signal is detected at a 45-GHz photodetector (PD) and its waveform is observed by a sampling oscilloscope (OSC). A power supply is used to provide a bias voltage applied to the MDR via a probe. As demonstrated,²³ for the implementation of a temporal differentiator, the phase response is

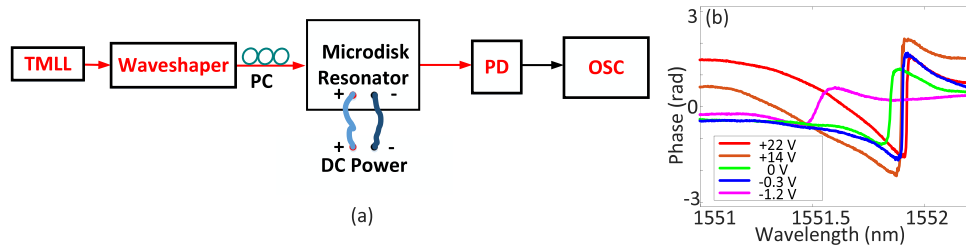


FIG. 7. (a) Experimental setup. TMLL: tunable mode lock laser, PC: polarization controller, PD: photodetector, OSC: oscilloscope. (b) Measured phase responses of the resonance WGM_{0,38} at different bias voltages.

more important than the magnitude response. The magnitude response of an ideal temporal differentiator may not be exactly satisfied by using the transmission band of the disk resonance, but the phase response which plays a key role can be controlled to be identical to that required by an ideal temporal differentiator. Fig. 7(b) shows the phase responses of the resonance WGM_{0,38} at different bias voltages. By changing the bias voltage, the phase response is changed, which could be used to realize a temporal differentiator with a different differentiation order. Note that as the bias voltage is tuned, the resonance wavelength also shifts, which requires that the carrier wavelength of the input Gaussian pulse is re-aligned to the resonance wavelength to enable an effective differentiation.

The shaped pulse at the output of the Waveshaper is shown as solid line in Fig. 8(a). An ideal Gaussian pulse with an identical temporal width of 500 ps is also shown as dashed line in Fig. 8(a), for comparison. The experimentally generated input pulse is close to a Gaussian pulse with a slight deviation. A differentiated pulse is obtained at the output of the PD and the waveform is observed by the OSC. Figs. 8(b)–8(f) show a differentiated pulse with differentiation orders of $n = 0.38, 0.86, 1.03, 1.12, \text{ or } 1.53$, as solid lines. Simulated pulses at the output of an ideal differentiator are also shown in Figs. 8(b)–8(f), as dashed lines. As can be seen, a good agreement is achieved between the experimentally generated pulses and the simulated pulses, which confirms the effectiveness of the MDR as a temporal differentiator. The root mean square error (RMSE) in the worst case (Fig. 8(f)) is calculated to be 9%. It should be noted that the difference in the notch is caused mainly due to the limited bandwidth of the PD (45 GHz). In addition, the wavelength shift with the bias voltage change could be eliminated by incorporating a micro-heater in the MDR to introduce an opposite wavelength shift. Thus, a tunable fraction-order temporal differentiator with an unchanged resonance wavelength could be realized. Compared with a temporal differentiator using an MRR,⁹ a

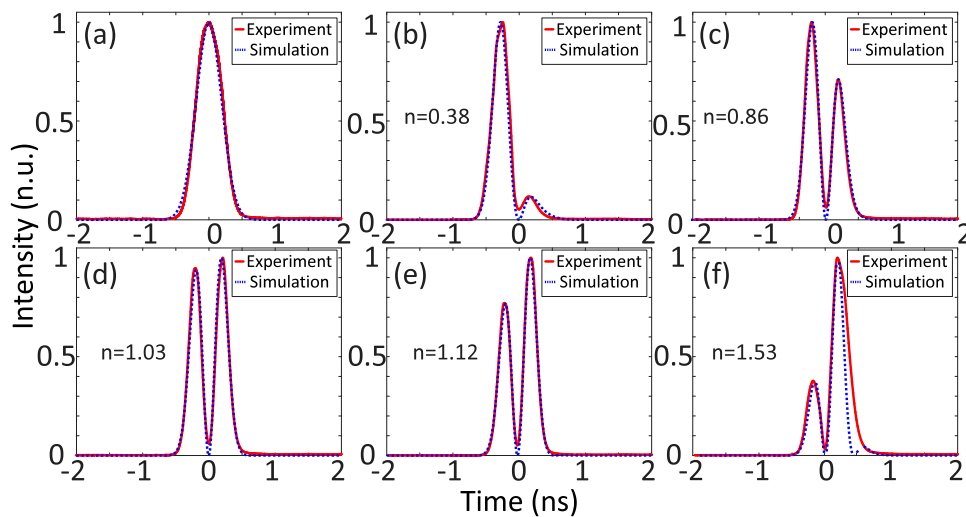


FIG. 8. Experimental results: (a) an input Gaussian pulse with an FWHM of 500 ps, and the differentiated pulses corresponding to a differentiation order of (b) $n = 0.38$, (c) $n = 0.86$, (d) $n = 1.03$, (e) $n = 1.12$, or (f) $n = 1.53$.

temporal differentiator using an MDR exhibits a larger tuning order with an ultra-compact footprint, which is highly needed in a more complicated signal processing system where the proposed MDR can be employed as a fundamental signal processing unit.

In conclusion, a novel silicon-based on-chip MDR was designed, fabricated, and evaluated and its applications for IMWP were investigated. By introducing a specifically designed slab waveguide to surround the disk and the lateral sides of the bus waveguide, the higher-order WGMs were suppressed. The adding of a slab waveguide also made it possible to incorporate a lateral PN junction, which was used for electrical tuning. An MDR based on the proposed design was fabricated and its optical performance was evaluated. The fabricated MDR exhibited a single-mode operation with a free spectral range of 28.85 nm. Its electrical tunability was also demonstrated and an electro-optic frequency response with a 3-dB modulation bandwidth as wide as ~ 30.5 GHz was achieved. The use of the fabricated MDR for the implementation of an electrically tunable optical delay-line and a tunable fractional-order temporal photonic differentiator was demonstrated.

The key features of the proposed silicon-based on-chip MDR include ultra-compact footprint, single-mode operation, no resonance-splitting, and flexible electrical tunability, which make the proposed MDR have a high potential for IMWP applications. In addition to the use of the proposed MDR for an electrically tunable optical delay-line and a tunable fractional-order photonic temporal differentiator, demonstrated in this paper, the design can also be used to achieve a wideband flat-top optical filter and a wideband optical delay line. For example, to realize a wideband flat-top optical filter, one may cascade multiple MDRs with specifically designed coupling gaps, to make the MDRs have slightly offset resonances. The same design using cascaded MDRs with specifically designed coupling gaps can also be applied to implement a wideband optical delay line. In addition, the proposed MDR could also act as a fundamental signal processing unit, to be employed in a more complicated signal processing system.

The work is supported by the Natural Sciences and Engineering Research Council of Canada under the Silicon Electronic-Photonic Integrated Circuits (Si-EPIC) CREATE program. We acknowledge CMC Microsystems, for providing the design tools and enabling the fabrication of the device.

- ¹ M. Hochberg and T. Baehr-Jones, "Silicon photonics," *Nat. Photonics* **4**, 492 (2010).
- ² D. Marpaung, C. Roeloffzen, R. Heideman, A. Leinse, S. Sales, and J. Capmany, "Integrated microwave photonics," *Laser Photonics Rev.* **7**, 1 (2013).
- ³ W. Zhang and J. P. Yao, "Silicon-based integrated microwave photonics," *IEEE J. Quantum Electron.* **52**, 0600412 (2016).
- ⁴ W. Bogaerts, P. De Heyn, T. Van Vaerenbergh, K. De Vos, S. Kumar Selvaraja, T. Claes, P. Dumon, P. Bienstman, D. Van Thourhout, and R. Baets, "Silicon microring resonators," *Laser Photonics Rev.* **6**, 47 (2012).
- ⁵ F. Liu, T. Wang, L. Qiang, T. Ye, Z. Zhang, M. Qiu, and Y. Su, "Compact optical temporal differentiator based on silicon microring resonator," *Opt. Express* **16**, 15880 (2008).
- ⁶ F. Liu, Q. Li, Z. Zhang, M. Qiu, and Y. Su, "Optically tunable delay line in silicon microring resonator based on thermal nonlinear effect," *IEEE J. Sel. Top. Quantum Electron.* **14**, 706 (2008).
- ⁷ F. Xia, L. Sekaric, and Y. A. Vlasov, "Ultracompact optical buffers on a silicon chip," *Nat. Photonics* **1**, 65 (2007).
- ⁸ Q. Xu, B. Shmidt, S. Pradhan, and M. Lipson, "Micrometre-scale silicon electro-optic modulator," *Nature* **435**, 325 (2005).
- ⁹ A. Zheng, J. Dong, L. Zhou, X. Xiao, Q. Yang, X. Zhang, and J. Chen, "Fractional-order photonic differentiator using an on-chip microring resonator," *Opt. Lett.* **39**, 6355 (2014).
- ¹⁰ M. Soltani, S. Yegnanarayanan, and A. Adibi, "Ultra-high Q planar silicon microdisk resonators for chip-scale silicon photonics," *Opt. Express* **15**, 4694 (2007).
- ¹¹ W. Shi, H. Yun, W. Zhang, C. Lin, T. K. Chang, Y. Wang, N. Jaeger, and L. Chrostowski, "Ultra-compact, high-Q silicon microdisk reflectors," *Opt. Express* **20**, 21840 (2012).
- ¹² J. Lloret, G. Morthier, F. Ramos, S. Sales, D. Thourhout, T. Spuesens, N. Olivier, J. Fédéli, and J. Capmany, "Broadband microwave photonic fully tunable filter using a single heterogeneously integrated III-V/SOI-microdisk-based phase shifter," *Opt. Express* **20**, 10796 (2012).
- ¹³ L. Liu, T. Yang, S. Liao, and J. Dong, "Photonic generation of millimeter-wave using a silicon microdisk resonator," *Opt. Commun.* **343**, 115 (2015).
- ¹⁴ L. Liu, F. Jiang, S. Yan, S. Min, M. He, D. Gao, and J. Dong, "Photonic measurement of microwave frequency using a silicon microdisk resonator," *Opt. Commun.* **335**, 266 (2015).
- ¹⁵ M. R. Watts, W. Zortman, D. Trotter, R. Young, and A. Lentine, "Vertical junction silicon microdisk modulators and switches," *Opt. Express* **19**, 21989 (2011).
- ¹⁶ L. Zhou and A. W. Poon, "Silicon electro-optic modulators using p-i-n diodes embedded 10-micron-diameter microdisk resonators," *Opt. Express* **14**, 6851 (2006).
- ¹⁷ F. Xia, M. Rooks, L. Sekaric, and Y. Vlasov, "Ultra-compact high order ring resonator filters using submicron silicon photonic wires for on-chip optical interconnects," *Opt. Express* **15**, 11934 (2007).

- ¹⁸ W. Zhang, N. Ehteshami, W. Liu, and J. P. Yao, "Silicon-based on-chip electrically tunable sidewall-Bragg-grating Fabry-Perot filter," *Opt. Lett.* **40**, 3153 (2015).
- ¹⁹ G. T. Reed, G. Mashanovich, F. Y. Gardes, and D. J. Thomson, "Silicon optical modulators," *Nat. Photonics* **4**, 518 (2010).
- ²⁰ T. Kato and Y. Kokubun, "Bessel-Thompson filter using double-series-coupled microring resonator," *J. Lightwave Technol.* **26**, 3694 (2008).
- ²¹ J. Azaña, "Ultrafast analog all-optical signal processors based on fiber-grating devices," *IEEE Photonics J.* **2**, 359 (2010).
- ²² C. Cuadrado-Laborde and M. V. Andres, "In-fiber all-optical fractional differentiator," *Opt. Lett.* **34**, 833 (2009).
- ²³ M. Li, L. Shao, J. Albert, and J. P. Yao, "Continuously tunable photonic fractional temporal differentiator based on a tilted fiber Bragg grating," *IEEE Photonics Technol. Lett.* **23**, 251 (2011).